PASJ: Publ. Astron. Soc. Japan **65**, 120, 2013 December 25

Low-Resolution Spectrum of the Diffuse Galactic Light and 3.3 μm PAH Emission with the AKARI InfraRed Camera

Kohji TSUMURA,[1] Toshio MATSUMOTO,[1,2] Shuji MATSUURA,[1] Itsuki SAKON,[3] Masahiro TANAKA,[4] and Takehiko WADA[1]
[1]*Department of Space Astronomy and Astrophysics, Institute of Space and Astronautical Science, Japan Aerospace Exploration Agency, 3-1-1 Yoshinodai, Chuo-ku, Sagamihara 252-5210*
tsumura@ir.isas.jaxa.jp
[2]*Institute of Astronomy and Astrophysics, Academia Sinica, No. 1, Roosevelt Rd, Sec. 4, Taipei 10617, Taiwan, R.O.C.*
[3]*Department of Astronomy, Graduate School of Science, The University of Tokyo, 7-3-1 Hongo, Bunkyo-ku, Tokyo 113-0033*
[4]*Center for Computational Sciences, University of Tsukuba, 1-1-1 Tennodai, Tsukuba, Ibaraki 305-8577*

(Received 2013 January 30; accepted 2013 July 25)

Abstract

We first obtained the spectrum of the diffuse Galactic light (DGL) at general interstellar space in the 1.8–5.3 μm wavelength region with the low-resolution prism spectroscopy mode of the AKARI Infra-Red Camera (IRC) NIR channel. The 3.3 μm PAH band is detected in the DGL spectrum at Galactic latitude $|b| < 15°$, and its correlations with the Galactic dust and gas are confirmed. The correlation between the 3.3 μm PAH band and the thermal emission from the Galactic dust is expressed not by a simple linear correlation, but by a relation with extinction. Using this correlation, the spectral shape of DGL at an optically thin region ($5° < |b| < 15°$) was derived as a template spectrum. Assuming that the spectral shape of this template spectrum is uniform at any position, the DGL spectrum can be estimated by scaling this template spectrum using the correlation between the 3.3 μm PAH band and the thermal emission from the Galactic dust.

Key words: infrared: ISM — ISM: dust, extinction — ISM: general — ISM: lines and bands

1. Introduction

Diffuse Galactic Light (DGL) comprises scattered starlight by dust particles in interstellar space at $< 3\,\mu$m, and emissions from the dust particles with some band features at longer wavelengths.[1] Thus, observational studies of DGL are important to investigate the dust property in our Galaxy, and it is also important for deriving the extragalactic background light (EBL), since DGL is one of the foregrounds for the EBL measurement. However, the isolation of DGL from other diffuse emissions, especially the strongest zodiacal light (ZL) foreground, is very difficult due to its diffuse, extended nature. A commonly used method to estimate DGL is the correlation with the dust column density estimated by the thermal emission of dust from far-infrared (100 μm) observations, or the column density of H I and/or CO from radio observations. At optical wavelengths, the DGL brightness (Witt et al. 2008; Matsuoka et al. 2011; Ienaka et al. 2013) and spectrum (Brandt & Draine 2012) are obtained by the correlation with the 100 μm dust thermal emission. However, observations of DGL at near-infrared (NIR) are limited and controversial.

The presence of infrared band features in DGL was first confirmed for the 3.3 μm band by the AROME balloon experiment (Giard et al. 1988). Such ubiquitous Unidentified Infrared (UIR) bands are a series of distinct emission bands seen at 3.3, 5.3, 6.2, 7.7, 8.6, 11.2, and 12.7 μm, and they are supposed to be carried by polycyclic aromatic hydrocarbons (PAH) (Leger & Puget 1984; Allamandola et al. 1985). They are excited by absorbing a single ultraviolet (UV) photon, and release the energy with a number of infrared photons in cascade via several lattice vibration modes of aromatic C–H and C–C bonds (Allamandola et al. 1989a). The 3.3 μm PAH band emission has been assigned to the stretching mode transition ($v = 1$–0) of the C–H bond on aromatic rings. There is a quantitative model for DGL from interstellar dust including PAH (Li & Draine 2001). The correlation between the 3.3 μm PAH band detected by the Near-Infrared Spectrometer (NIRS) on the Infrared Telescope in Space (IRTS) and the 100 μm thermal emission of the large dust grains by the Infrared Astronomical Satellite (IRAS) was confirmed at the Galactic plane region ($42° < l < 55°$, $|b| < 5°$), implying that the PAH molecules are well mixed with large dust grains at the Galactic plane (Tanaka et al. 1996).

In this paper, we describe the DGL spectrum obtained with the low-resolution prism spectroscopy mode on the AKARI Infra-Red Camera (IRC) NIR channel in the 1.8–5.3 μm wavelength region. Our idea to derive the DGL spectrum at NIR in this paper is to use the 3.3 μm PAH band feature as a tracer of DGL combined with the correlation with the 100 μm dust thermal emission. The 3.3 μm PAH band is detected in this wavelength region at $|b| < 15°$, and the correlation with the thermal emission of large dust grains is also confirmed. Using this correlation, we developed a method to estimate the DGL spectrum at NIR at any location.

This paper is organized as follows. In section 2, we describe the data reduction. In section 3, we describe the correlation of the 3.3 μm PAH band feature in DGL with Galactic latitude and the distribution of Galactic dust and gas. The method to estimate DGL spectrum using this correlation is shown in

[1] Although the term DGL sometimes indicates only the scattered starlight component, the term DGL indicates both scattered starlight and emission components in this paper.

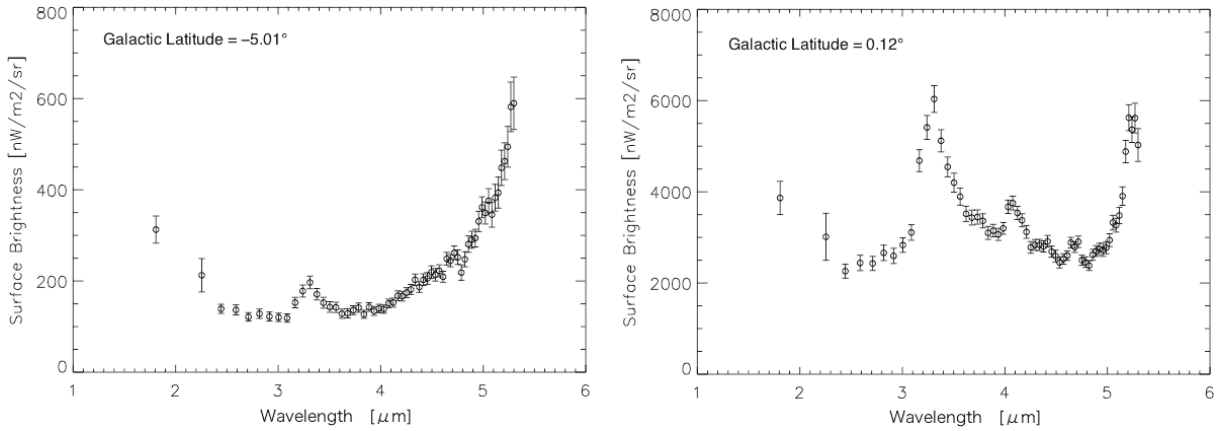

Fig. 1. Examples of the diffuse sky spectra obtained with AKARI IRC. (a) Spectrum at $b = -5°$. The 3.3 μm PAH band is clearly visible on the bottom of the ZL spectrum. (b) Spectrum at the Galactic plane. DGL dominates the sky brightness and strong PAH bands at 3.3 μm and 5.25 μm and Brα at 4.1 μm are clearly visible.

section 4, and a summary of this paper is given in section 5. There are two companion papers describing the spectrum of the infrared diffuse sky; ZL is described in Tsumura et al. (2013a, hereafter Paper I), and EBL is described in Tsumura et al. (2013b, hereafter Paper III) in which the foregrounds described in Paper I and this paper (Paper II) are subtracted.

2. Data Selection and Reduction

AKARI is the first Japanese infrared astronomical satellite launched in 2006 February, equipped with a cryogenically cooled telescope of 68.5 cm aperture diameter (Murakami et al. 2007). IRC is one of two astronomical instruments of AKARI, and it covers the 1.8–5.3 μm wavelength region with a 512 × 412 InSb detector array in the NIR channel[2] (Onaka et al. 2007). It provides low-resolution ($\lambda/\Delta\lambda \sim 20$) slit spectroscopy for diffuse radiation by a prism[3] (Ohyama et al. 2007). One of the biggest advantage compared to the previous IRTS measurement (Tanaka et al. 1996) is the higher angler resolution (1.″46) of AKARI IRC, which allows us to detect and remove fainter point sources, while the IRTS measurement was highly contaminated by bright stars at the Galactic plane because of its resolution (8′).

See Paper I for details of the data selection and reduction. Here, we simply note that 278 pointed data of diffuse spectrum were selected in this study, distributing a wide range of ecliptic and Galactic coordinates. The dark current was subtracted by a method specialized for diffuse sky analysis, described in Tsumura and Wada (2011). Stars brighter than m_K(Vega) = 19 were detected on the slit and masked for deriving the diffuse spectrum. It was confirmed that the brightness due to unresolved Galactic stars under this detection limit is negligible (< 0.5% of the sky brightness at 2.2 μm) by a Milky Way star counts model, TRILEGAL (TRIdimensional modeL of thE GALaxy: Girardi et al. 2005). The cumulative brightness contributed by unresolved galaxies can be estimated by the deep galaxy counts, being $< 4\,\mathrm{nW\,m^{-2}\,sr^{-1}}$ at the K band in the case of a limiting magnitude of $m_K = 19$ (Keenan et al. 2010).

3. 3.3 μm PAH Band

3.1. Association to Our Galaxy

Figure 1 shows examples of the spectra of the infrared diffuse sky used in this study. Although the obtained spectra are dominated by ZL except for the Galactic plane, the 3.3 μm PAH band is detectable at $|b| < 15°$ in our dataset. The 3.3 μm PAH band is easy to be found at the bottom of the ZL spectrum, because the ZL spectrum has a local minimum at around 3.5 μm, as shown in figure 1a. At the Galactic plane, DGL dominates the sky spectrum, as shown in figure 1b. The spectral shape of the 3.3 μm band is asymmetric because other 3.4 and 3.5 μm PAH sub-band features are combined and detected together, which were separately detected by high-resolution spectroscopy ($\lambda/\Delta\lambda \sim 120$) with the IRC grism mode at the Galactic plane (Onaka et al. 2011).

The 3.3 μm PAH band was extracted from the sky spectrum by almost the same method as that used in Tanaka et al. (1996). First, the continuum intensity at 3.3 μm ($\lambda I^{\mathrm{cont}}_{3.3\mu\mathrm{m}}$) was interpolated between 3.2 and 3.8 μm. Although the continuum was interpolated between 3.2 and 3.6 μm in Tanaka et al. (1996), we used the intensity at 3.8 μm for the interpolation to avoid contamination from the PAH sub-feature at 3.5 μm. Then, the total energy of the 3.3 μm PAH band feature ($E_{3.3}$) was calculated as the excess from the continuum,

$$E_{3.3} = \frac{\Delta\lambda}{\lambda}\left(\lambda I_{3.3\mu\mathrm{m}} - \lambda I^{\mathrm{cont}}_{3.3\mu\mathrm{m}}\right) + 0.58, \quad (1)$$

where $\Delta\lambda = 0.13\,\mu$m was employed for a direct comparison to Tanaka et al. (1996), and two data points around 3.3 μm were summed to compute $\lambda I_{3.3\mu\mathrm{m}}$ for matching the wavelength resolution to IRTS and reducing the error. A small offset of $0.58\,\mathrm{nW\,m^{-2}\,sr^{-1}}$ was applied to correct the difference between the ZL continuum and the linear interpolation

[2] IRC has two other channels covering 5.8–14.1 μm in the MIR-S channel and 12.4–26.5 μm in the MIR-L channel.

[3] High-resolution spectroscopy ($\lambda/\Delta\lambda \sim 120$) with a grism is also available.

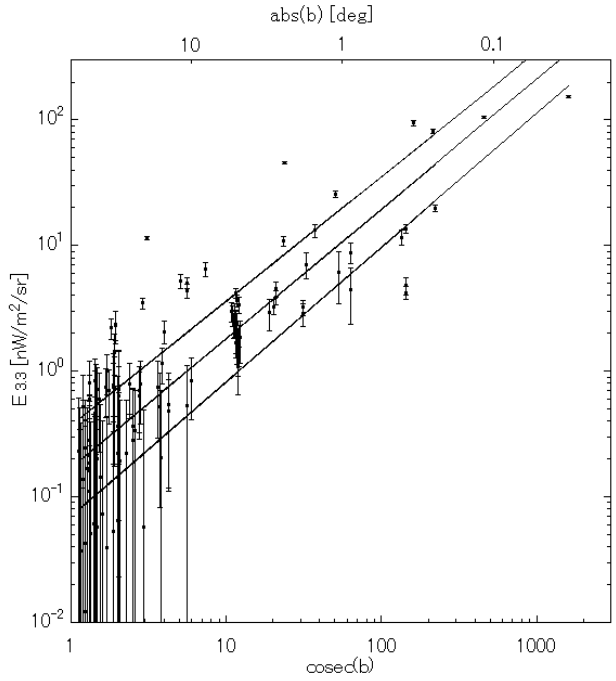

Fig. 2. Correlation of the 3.3 μm PAH band intensity ($E_{3.3}$) to the Galactic latitude (b). The solid lines are the best-fit lines to the data.

between 3.2 and 3.8 μm. The PAH band at $| b | < 15°$ was detected by this method.

First, we show a general correlation of this PAH band with our Galaxy in figure 2. This means that the PAH dust is associated with DGL from our Galaxy, and this correlation can be expressed by

$$E_{3.3} = (0.17^{+0.2}_{-0.1}) \times (\mathrm{cosec} \mid b \mid)^{(1.03 \mp 0.04)}. \quad (2)$$

Since such a correlation between the 3.3 μm PAH band and the ecliptic latitude was not detected, we can conclude that the observed PAH features are not associated with ZL from the Solar system.

3.2. Association to the Distribution of Dust and Gas

Next, we tested the correlations of the PAH band with the distribution of Galactic dust and gas, which are not correlated simply with the Galactic latitude. The 100 μm intensity map ($\lambda I_{100\mu\mathrm{m}}$), which is a reprocessed composite of the COBE/DIRBE and IRAS/ISSA maps (SFD map, see Schlegel et al. 1998), is used as the dust distribution, and the column density map of H I obtained from the Leiden/Argentine/Bonn (LAB) Galactic H I survey (Kalberla et al. 2005) is used as the gas distribution map. The good correlation between the dust and gas was reported (Stark et al. 1992; Arendt et al. 1998), and the H I column density can be converted to the 100 μm intensity by 0.018 ± 0.003 (μW m^{-2} sr^{-1})/(10^{20} atoms cm^{-2}) at $N_{\mathrm{H}} < 10^{22}$ atoms cm^{-2}, as adopted in Matsuura et al. (2011). In previous studies, the correlation between the 3.3 μm PAH band and the 100 μm thermal intensity was reported by Giard et al. (1989) and Tanaka et al. (1996), but they were limited at the Galactic plane ($| b | < 6°$). The AKARI data in this study provide correlations up to $| b | = 15°$ with higher angler resolution and higher sensitivity of point sources to remove foreground stars than that in previous works.

Figure 3 shows the correlations of the 3.3 μm PAH band of our data set with the 100 μm thermal intensity from the SFD map (Schlegel et al. 1998) and the column density of H I from the LAB survey (Kalberla et al. 2005). These correlations can be expressed by

$$\frac{E_{3.3}}{\mathrm{nW\,m^{-2}\,sr^{-1}}} = (2.9 \pm 1.0) \times \left(\frac{\lambda I_{100\mu\mathrm{m}}}{\mu\mathrm{W\,m^{-2}\,sr^{-1}}} \right)^{(0.91 \mp 0.04)}, \quad (3)$$

$$\frac{E_{3.3}}{\mathrm{nW\,m^{-2}\,sr^{-1}}} = (0.7 \pm 0.3) \times \left(\frac{N_{\mathrm{H}}}{10^{21}\,\mathrm{atoms\,cm^{2}}} \right)^{(1.08 \mp 0.05)}. \quad (4)$$

These correlations are better than the correlation with the Galactic latitude shown in figure 2, which means that PAH molecules, interstellar dust, and interstellar gas are well mixed in interstellar space. The deviation of the correlation with N_{H} in the LAB survey data shown in figure 3b is larger than the correlation with the 100 μm intensity in SFD map shown in figure 3a, because the angular resolution of the SFD map is better than the LAB map, allowing us better point-to-point correlation analysis. Thus, the advanced analysis described in the next sub-section is investigated only for the correlation with the 100 μm intensity.

3.3. The Effect of Extinction on the PAH Band

Tanaka et al. (1996) assumed a simple linear relation between $E_{3.3}$ and $\lambda I_{100\mu\mathrm{m}}$, obtaining a relation of $E_{3.3}/\lambda I_{100\mu\mathrm{m}} = (2.9 \pm 0.9) \times 10^{-3}$; also, the systematic difference from the linear relation at the high $\lambda I_{100\mu\mathrm{m}}$ region was concluded to be due to extinction. Giard et al. (1989) also investigated the correlation between $E_{3.3}$ and $\lambda I_{100\mu\mathrm{m}}$, and found the extinction at the Galactic plane. The power of 0.91 ∓ 0.04 (smaller than unity) in our fitting in equation (3) is consistent with the extinction as mentioned in Giard et al. (1989) and Tanaka et al. (1996). Therefore, we conducted a fitting that included the effect of extinction.

When the source's term in the transfer equation is proportional to the extinction term all along the line of sight, the extinction can be written as $(1 - e^{-\tau_\lambda})/\tau_\lambda$, where τ_λ is the optical depth at wavelength λ (Giard et al. 1989). Then, the correlation with the extinction between the PAH emission ($E_{3.3}$) and the the 100 μm intensity ($\lambda I_{100\mu\mathrm{m}}$) can be written as

$$\frac{E_{3.3}}{\mathrm{nW\,m^{-2}\,sr^{-1}}} = \alpha \frac{1 - e^{-\tau_{3.3}}}{\tau_{3.3}} \left(\frac{\lambda I_{100\mu\mathrm{m}}}{\mu\mathrm{W\,m^{-2}\,sr^{-1}}} \right), \quad (5)$$

where α is a fitting parameter. Assuming that the 100 μm intensity is proportional to the number of PAH molecules associated with dust particles, and the number of dust particles is proportional to $\tau + \tau^2$ (Rybicki & Lightman 1986), the optical depth $\tau_{3.3}$ can be obtained as a solution of

$$\frac{\lambda I_{100\mu\mathrm{m}}}{\mu\mathrm{W\,m^{-2}\,sr^{-1}}} = \frac{1}{\beta}(\tau_{3.3} + \tau_{3.3}^2), \quad (6)$$

where β is another fitting parameter. By fitting to our data, we obtained $\alpha = 3.5 \pm 1.0$ and $\beta = 0.10 \pm 0.04$. The curve of

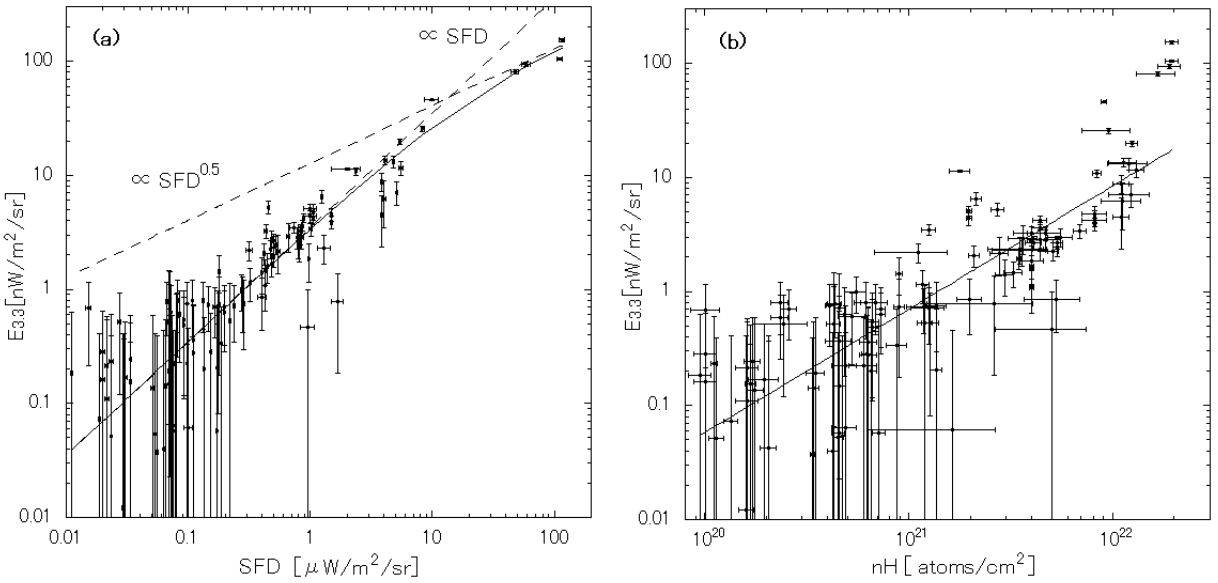

Fig. 3. Correlation of the PAH 3.3 μm band intensity with (a) the 100 μm intensity from the SFD map (Schlegel et al. 1998) and (b) column density of H I from the LAB survey (Kalberla et al. 2005). Best-fit curves of equation (5) for panel (a) and equation (4) for panel (b) are also shown by solid curves. Two extreme cases of $\propto SFD$ and $\propto \sqrt{SFD}$ are also shown by broken lines in panel (a).

equation (5) with best-fit parameters is shown as a solid curve in figure 3a.

In the optically thin case ($\tau_{3.3} \ll 1$), the extinction term, $(1 - e^{-\tau_{3.3}})/\tau_{3.3}$, becomes unity. We thus obtain a linear correlation,

$$\frac{E_{3.3}}{\mathrm{nW\,m^{-2}\,sr^{-1}}} = \alpha \left(\frac{\lambda I_{100\mu\mathrm{m}}}{\mu\mathrm{W\,m^{-2}\,sr^{-1}}} \right) \quad (\tau_{3.3} \ll 1). \tag{7}$$

In the optically thick case ($\tau_{3.3} \gg 1$), the extinction term can be written as $1/\tau_{3.3}$, because the term $e^{-\tau_{3.3}}$ becomes zero. In addition, the optical depth, $\tau_{3.3}$, can be written as $\tau_{3.3} = \sqrt{\beta \times \lambda I_{100\mu\mathrm{m}}}$ from equation (6) owing to $\tau_{3.3} \gg 1$. Combining these equations, we obtain

$$\frac{E_{3.3}}{\mathrm{nW\,m^{-2}\,sr^{-1}}} = \frac{\alpha}{\sqrt{\beta}} \sqrt{\frac{\lambda I_{100\mu\mathrm{m}}}{\mu\mathrm{W\,m^{-2}\,sr^{-1}}}} \quad (\tau_{3.3} \gg 1). \tag{8}$$

These two extreme cases are also shown as broken lines in figure 3a.

The gradient of $\alpha = 3.5 \pm 1.0$ is higher than the value from the IRAS result of $\alpha = 2.5 \pm 0.4$ (Giard et al. 1994), but this result was determined based on the data averaged in the Galactic latitude range of $| b | < 1°$, where bright discrete sources were included. IRTS, with higher sensitivity than IRAS, but still limited at $| b | < 5°$, obtained a value of $\alpha = 2.9 \pm 0.9$ in Tanaka et al. (1996), which is closer to our result. The 3.3 μm PAH band intensity deviates from linearity at $\lambda I_{100\mu\mathrm{m}} > 10\,\mu\mathrm{W\,m^{-2}\,sr^{-1}}$ or $| b | < 1°$. This is equivalent to $\tau_{3.3} = 0.6$ at $\lambda I_{100\mu\mathrm{m}} > 10\,\mu\mathrm{W\,m^{-2}\,sr^{-1}}$ or $| b | < 1°$ in our fitting, which is higher than the estimated value of $\tau_{3.3} = 0.18$ at $| b | < 0.°75$ based on the extinction law summarized in Mathis (1990) and the optical depth at 240 μm from Sodroski et al. (1994).

4. DGL Spectrum

4.1. Correlation Method

In this section, we develop a method to derive the DGL spectrum at 1.8–5.3 μm by the correlation with the 100 μm intensity. The diffuse sky spectrum includes ZL, DGL, and EBL, i.e.,

$$SKY(\lambda) = ZL(\lambda) + DGL(\lambda) + EBL(\lambda). \tag{9}$$

ZL is modeled in Paper I, which can be subtracted based on the DIRBE ZL model (Kelsall et al. 1998), and EBL is the isotropic component. Therefore, only DGL has a correlation with the 100 μm intensity, so DGL can be derived by the correlation by assuming a linear correlation with the 100 μm intensity,

$$SKY(\lambda) - ZL(\lambda) = a(\lambda) \times \lambda I_{100\mu\mathrm{m}} + b(\lambda), \tag{10}$$

where $a(\lambda) \times \lambda I_{100\mu\mathrm{m}}$ is equivalent to $DGL(\lambda)$ and $b(\lambda)$ is equivalent to $EBL(\lambda)$. Figure 4 shows the correlation between $SKY(\lambda) - ZL(\lambda)$ in our dataset and the 100 μm intensity from the SFD map (Schlegel et al. 1998). The data for this correlation analysis were selected by a criteria of $\lambda I_{100\mu\mathrm{m}} < 3\,\mu\mathrm{W\,m^{-2}\,sr^{-1}}$, equivalent to the Galactic latitude $| b | > 5°$, to trace low dust density regions owing to the assumption of a linear correlation. The gradients as a function of the wavelength in figure 4, $a(\lambda)$, correspond to the spectral shape of DGL. Normalized spectrum of the obtained DGL spectrum is shown in figure 5a, and the 3.3 μm PAH band feature in DGL was detected. The error of the obtained DGL spectrum by this correlation method is 5% at $< 3.8\,\mu$m, 15% between 3.8 μm and 4.2 μm, and 20% at $> 4.2\,\mu$m. Since the spectral shape of DGL may vary depending on the environments, it is a representative spectrum of DGL at low dust density regions, typically

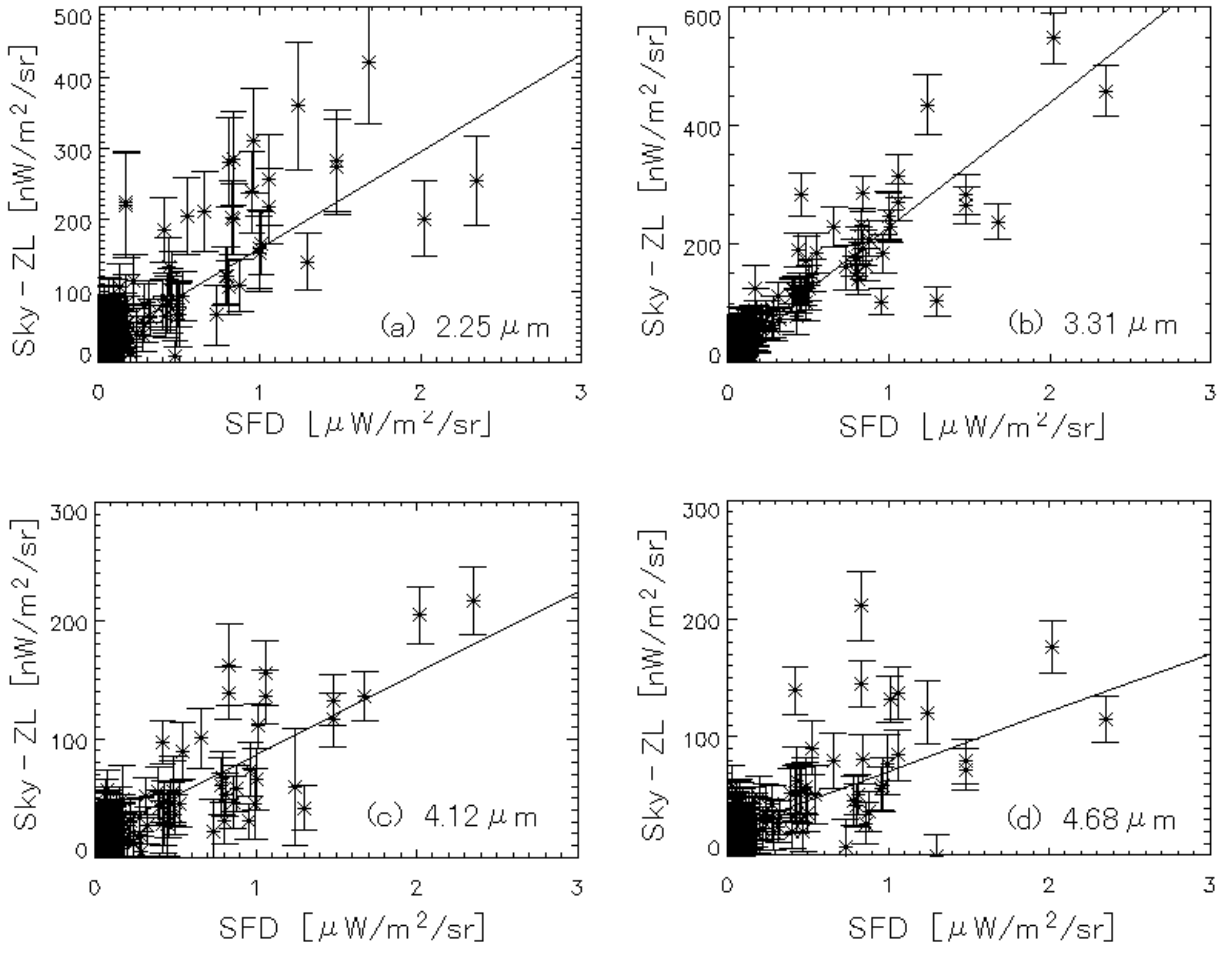

Fig. 4. Examples of correlation between $SKY(\lambda) - ZL(\lambda)$ and the 100 μm intensity in the SFD map at $\lambda I_{100\mu\mathrm{m}} < 3\,\mathrm{nW\,m^{-2}\,sr^{-1}}$ at (a) 2.25 μm, (b) 3.31 μm, (c) 4.12 μm, and (d) 4.68 μm.

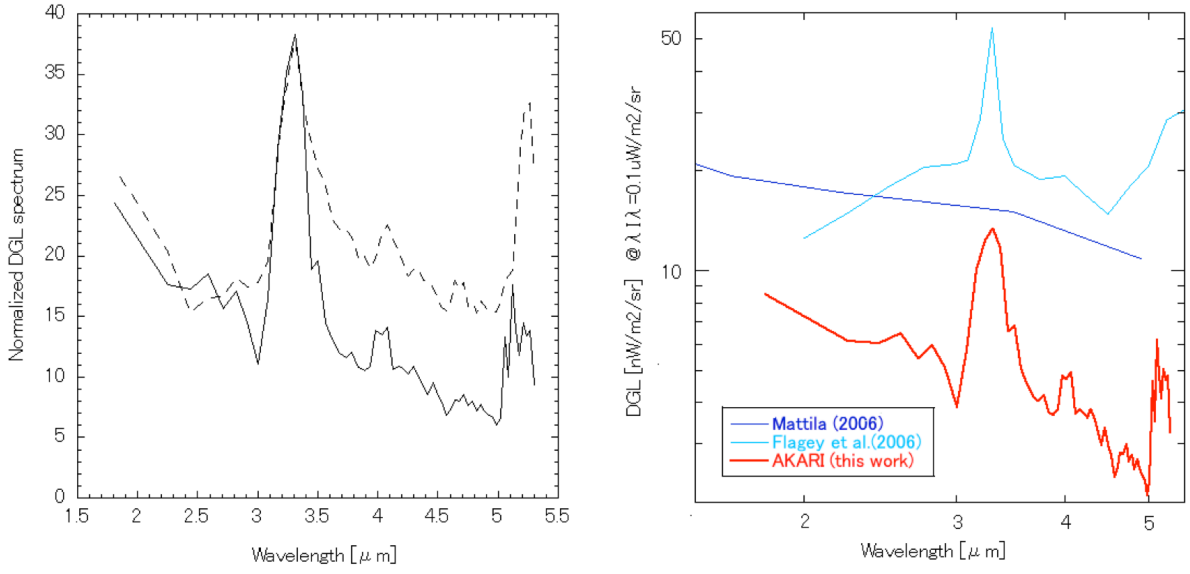

Fig. 5. (a) DGL template spectrum (solid curve) from the correlation of the data at $5^\circ < |\, b \,| < 15^\circ$ and the averaged spectrum at the Galactic plane (broken curve) normalized to be $E_{3.3} = 1$. The error of the obtained DGL spectrum by this correlation method is 5% at $< 3.8\,\mu$m, 15% between 3.8 μm and 4.2 μm, and 20% at $> 4.2\,\mu$m. (b) DGL spectra scaling to $\lambda I_{100\mu\mathrm{m}} = 0.1\,\mu\mathrm{W\,m^{-2}\,sr^{-1}}$ or $N_{\mathrm{H}} = 5 \times 10^{20}\,\mathrm{atoms\,cm^{-2}}$ by our method and other estimations (Mattila 2006; Flagey et al. 2006).

Table 1. Selected regions at the Galactic plane for evaluating the DGL spectrum.

Pointing ID	Galactic longitude l (°)	Galactic latitude b (°)	$\lambda I_{100\mu m}$ (μW m^{-2} sr^{-1})	$N_{\rm H}$ (atoms cm^{-2})
410017.1	30.76	0.36	59.00	1.89×10^{22}
410018.1	31.01	0.12	111.09	1.95×10^{22}
410021.1	30.99	−0.04	115.25	1.95×10^{22}
410022.1	31.24	−0.27	47.65	1.66×10^{22}

$5^\circ < \mid b \mid < 15^\circ$; the variance of the environments is included in these errors.

In this correlation method, we assumed a linear correlation between DGL and the 100 μm intensity, but we have already shown the non-linear correlation between the 3.3 μm PAH band and the 100 μm intensity owing to extinction, as shown in figure 3a. Thus, we modify this DGL estimation method by combining it with the 3.3 μm PAH band as a tracer for scaling the DGL spectrum at any general sky. First, the template DGL spectrum $DGL_{\rm temp}(\lambda)$ is defined as the derived DGL spectrum by this correlation method normalized to be $E_{3.3} = 1$,

$$DGL_{\rm temp}(\lambda) = \frac{a(\lambda)}{E_{3.3}[a(\lambda)]}. \quad (11)$$

This template DGL spectrum is shown in figure 5a. Assuming that the spectral shape of this template DGL spectrum does not change at any location, we can estimate the DGL spectrum at any place by scaling this template DGL spectrum by $E_{3.3}$, which can be obtained as a function of the 100 μm thermal intensity using the correlation shown in figure 3a, i.e.,

$$DGL(\lambda) = E_{3.3}(I_{100\mu m}) \times DGL_{\rm temp}(\lambda). \quad (12)$$

Figure 5b shows the the resultant DGL spectrum with other DGL estimations (Mattila 2006; Flagey et al. 2006) scaling to $\lambda I_{100\mu m} = 0.1\,\mu$W m^{-2} sr^{-1} or $N_{\rm H} = 5 \times 10^{20}$ atoms cm^{-2}.

Our DGL spectrum is lower than the other previous estimations, but our method gives a better DGL estimation at the general interstellar space with low dust density. In previous works, DGL was estimated by scaling using $N_{\rm H}$ based on only a limited number of specific dense regions with $N_{\rm H} \sim 2 \times 10^{22}$ atoms cm^{-2}. However, the ratio of DGL/$N_{\rm H}$ at dense regions ($> 10^{22}$ atoms cm^{-2}) is higher than that in the general interstellar fields, as shown in figure 3b, which leads to high DGL estimations in previous works. On the other hand, our estimation is based on a number of the wide-spread data points at the general interstellar fields with low dust density and higher spacial resolution to remove stars. In addition, scaling is based on the 100 μm intensity, which has a tighter correlation to DGL, as shown in figure 3a. Therefore, our estimate gives a more reliable estimation of the DGL spectrum, especially at low dust density regions.

Although our DGL estimation is lower than previous estimations, it may still overestimate the 3.3 μm intensity at high Galactic latitude regions. The 3.3 μm PAH band was detected only at the region of $\mid b \mid < 15^\circ$ in our dataset, and we assumed that the obtained spectral shape of DGL does not change at any location in this method, but there is no guarantee that this assumption is valid at high Galactic latitude regions. For example, the UV radiation field at high Galactic latitude regions is weaker than that at the Galactic plane (Seon et al. 2011); therefore, the PAH molecules are less excited at high Galactic latitude than the Galactic plane. In such a case, our method overestimates the 3.3 μm intensity in DGL at high Galactic latitude, as implied in Paper III.

4.2. DGL Spectrum in the Galactic Plane

We compared the obtained DGL spectrum by the correlation method ($5^\circ < \mid b \mid < 15^\circ$) with the spectrum at the Galactic plane, because the diffuse sky spectrum at the Galactic plane is dominated by DGL. For example, the DGL brightness at the Galactic plane in this wavelength region is several thousand nW m^{-2} sr^{-1}, while the ZL brightness is a few hundred nW m^{-2} sr^{-1}, which is less than 5%, as shown in figure 1. Therefore, the spectral shape of DGL can be evaluated by the diffuse sky spectra at the Galactic plane. We selected four spectra with the strongest 100 μm dust thermal emission and H I column density in our data set, located at the Galactic plane (l, b) $\sim$ (31°, 0°) summarized in table 1, where the brightness of the ZL contribution is $< 5\%$. These spectra at the Galactic plane are similar to each other with $\sim 15\%$ dispersion. The broken curve in figure 5a shows the average spectrum of these selected spectra normalized to be $E_{3.3} = 1$. The 3.3 μm PAH band is the most distinctive among others, and the second outstanding feature at 5.25 μm is also the PAH feature (Allamandola et al. 1989b; Cohen et al. 1989; Boersma et al. 2009). Brα at 4.05 μm and Pfβ at 4.65 μm are also detected, which can be useful information to estimate the ionizing temperature and extinction. One example of such a study in the M17 case with AKARI IRC high-resolution spectroscopy mode ($\lambda/\Delta\lambda \sim 120$) can be found in Onaka et al. (2011).

An excess continuum emission at the Galactic plane was confirmed at $> 3.5\,\mu$m, as shown in figure 5a. This excess continuum emission was first reported in visual reflection nebulae (Sellgren et al. 1983), and then found in galaxies (Lu et al. 2003; Onaka et al. 2010) and DGL (Flagey et al. 2006). The emission process of this excess continuum is still unknown, but Flagey et al. (2006) suggested the PAH fluorescence excited by UV photons. This excess continuum emission may be a reason why previous studies overestimated DGL from high dust density regions, as shown in figure 5b.

5. Summary

The 3.3 μm PAH band is detected in the diffuse sky spectrum of the interstellar space at $\mid b \mid < 15^\circ$, and this band intensity is correlated with the 100 μm thermal intensity of interstellar dust and the H I column density. We modeled the correlation

between the 3.3 μm PAH band and the 100 μm thermal intensity with extinction. We also introduced a method to estimate the DGL spectrum at 1.8–5.3 μm. This is the first estimation of DGL spectrum in the general sky at NIR based on observations. In this method, the spectral shape of DGL is derived by the correlation with the 100 μm thermal intensity, and it is scaled by the correlation of the 3.3 μm PAH band brightness as a tracer. The DGL spectrum estimated by our method is lower than the previous estimations, but our result is more reliable for the regions with low dust density regions because it is based on a wide range of general interstellar fields, whereas previous results were based on some specific regions with high dust density. In addition, we found the excess continuum emission at the Galactic plane at 3–5 μm, as reported by previous studies.

This research is based on observations with AKARI, a JAXA project with the participation of ESA. This research is also based on significant contributions of the IRC team. We thank Dr. Mori-Ito Tamami (The University of Tokyo) and Mr. Arimatsu Ko (ISAS/JAXA) for discussion about PAH. The authors acknowledge support from Japan Society for the Promotion of Science, KAKENHI (grant numbers 21111004 and 24111717).

References

Allamandola, L. J., Bregman, J. D., Sandford, S. A., Tielens, A. G. G. M., Witteborn, F. C., Wooden, D. H., & Rank, D. 1989b, ApJ, 345, L59
Allamandola, L. J., Tielens, A. G. G. M., & Barker J. R. 1985, ApJ, 290, L25
Allamandola, L. J., Tielens, A. G. G. M., & Barker J. R. 1989a, ApJS, 71, 733
Arendt, R. G., et al. 1998, ApJ, 508, 74
Boersma, C., Mattioda, A. L., Bauschlicher, C. W., Peeters, E., Tielens, A. G. G. M., & Allamandola, L. J. 2009, ApJ, 690, 1208
Brandt, T. D., & Draine, B. T. 2012, ApJ, 744, 129
Cohen, M., Tielens, A. G. G. M., Bregman, J. D., Witteborn, F. C., Rank, D. M., Allamandola, L. J., Wooden, D. H., & de Muizon, M. 1989, ApJ, 341, 246
Flagey, N., Boulanger, F., Verstraete, L., Miville Deschênes, M. A., Noriega Crespo, A., & Reach, W. T. 2006, A&A, 453, 969
Giard, M., Lamarre, J. M., Pajot, F., & Serra, G. 1994, A&A, 286, 203
Giard, M., Pajot, F., Lamarre, J. M., Serra, G., & Caux, E. 1989, A&A, 215, 92
Giard, M., Pajot, F., Lamarre, J. M., Serra, G., Caux, E., Gispert, R., Léger, A., & Rouan, D. 1988, A&A, 201, L1
Girardi, L., Groenewegen, M. A. T., Hatziminaoglou, E., & da Costa, L. 2005, A&A, 436, 895
Ienaka, N., Kawara, K., Matsuoka, Y., Sameshima, H., Oyabu, S., Tsujimoto, T., & Peterson, B. A. 2013, ApJ, 767, 80
Kalberla, P. M. W., Burton, W. B., Hartmann, D., Arnal, E. M., Bajaja, E., Morras, R., & Pöppel, W. G. L. 2005, A&A, 440, 775
Keenen, R. C., Barger, A. J., Cowie, L. L., & Wang, W.-H. 2010, ApJ, 723, 40
Kelsall, T., et al. 1998, ApJ, 508, 44
Leger, A., & Puget, J. L. 1984, A&A, 137, L5
Li, A., & Draine, B. T. 2001, ApJ, 554, 778
Lu, N., et al. 2003, ApJ, 588, 199
Mathis, J. S. 1990, ARA&A, 28, 37
Matsuoka, Y., Ienaka, N., Kawara, K., & Oyabu, S. 2011, ApJ, 736, 119
Matsuura, S., et al. 2011, ApJ, 737, 2
Mattila, K. 2006, MNRAS, 372, 1253
Murakami, H., et al. 2007, PASJ, 59, S369
Ohyama, Y., et al. 2007, PASJ, 59, S411
Onaka, T., et al. 2007, PASJ, 59, S401
Onaka, T., Matsumoto, H., Sakon, I., & Kaneda, H. 2010, A&A, 514, A15
Onaka, T., Sakon, I., Ohsawa, R., Shimonishi, T., Okada, Y., Tanaka, M., & Kaneda, H. 2011, in PAHs and the Universe: A Symp. to Celebrate 25th Anniversary of the PAH Hypothesis, ed. C. Joblin & A. G. G. M. Tielens (Cambridge, UK: Cambridge University Press), 55
Rybicki, G. B., & Lightman, A. P. 1986, Radiative Processes in Astrophysics (New York: Wiley)
Schlegel, D. J., Finkbeiner, D. P., & Davis, M. 1998, ApJ, 500, 525
Sellgren, K., Werner, M. W., & Dinerstein, H. L. 1983, ApJ, 271, L13
Seon, K.-I., et al. 2011, ApJS, 196, 15
Sodroski, T. J., et al. 1994, ApJ, 428, 638
Stark, A. A., Gammie, C. F., Wilson, R. W., Balley, J., Linke, R. A., Heiles, C., & Hurwitz, M. 1992, ApJS, 79, 77
Tanaka, M., Matsumoto, T., Murakami, H., Kawada, M., Noda, M., & Matsuura, S. 1996, PASJ, 48, L53
Tsumura, K., Matsumoto, T., Matsuura, J., Pyo, S., Sakon, I., & Wada, T. 2013a, PASJ, 65, 119 (Paper I)
Tsumura, K., Matsumoto, T., Matsuura, S., Sakon, I., & Wada, T. 2013b, PASJ, 65, 121 (Paper III)
Tsumura, K., & Wada, T. 2011, PASJ, 63, 755
Witt, A. N., Mandel, S., Sell, P. H., Dixon, T., & Vijh, U. P. 2008, ApJ, 679, 497